Skyrmions and multisublattice helical states in a frustrated chiral magnet

H. Y. Yuan,[1,2,*] O. Gomonay,[1,3,†] and Mathias Kläui[1]

[1]*Institut für Physik, Johannes Gutenberg-Universität Mainz, 55099 Mainz, Germany*

[2]*Department of Physics, Southern University of Science and Technology, Shenzhen, 518055 Guangdong, China*

[3]*National Technical University of Ukraine "KPI", 03056 Kyiv, Ukraine*

(Received 7 October 2016; revised manuscript received 30 August 2017; published 12 October 2017)

We show that frustrated exchange interactions could stabilize chiral states in a chiral ferromagnet by considering the competition between ferromagnetic (FM) nearest-neighbor (NN) interaction and antiferromagnetic (AFM) next-nearest-neighbor (NNN) interaction. In the low-field regime, a multisublattice helical state is found, which is different from the normal one-sublattice helical states in a FM and the two-sublattice helical states in a two-sublattice AFM. As the field increases further, the skyrmion lattice is even stable with a much larger energy-preferable window than a system without frustration. We argue that the enlargement of the stability window of skyrmions is a consequence of the reduced effective exchange interaction caused by the frustration. As a byproduct, the hysteresis loop of the frustrated chiral system shrinks as the magnetization goes to zero and then opens up again, which is known as the wasp-waist hysteresis loop. The critical field that separates the narrow and wide part of the wasp-waist loop depends exponentially on the strength of NNN coupling. Our results provide physical insight into the chiral states in the magnetic systems with the coexistence of frustrated exchange and chiral interaction and might even prove important for novel devices, where the stability window of skyrmions is a key asset.

DOI: 10.1103/PhysRevB.96.134415

I. INTRODUCTION

Skyrmions are topologically protected spin structures and are promising information carriers in spintronics because they have smaller size and can be manipulated using low current density [1]. Skyrmions in a magnetic system are first predicted theoretically [2–4] and then realized in the bulk magnets with noncentrosymmetric structures [5] and in the thin films with broken inversion symmetry [6–8]. The existence of Dzyaloshinskii-Moriya interaction (DMI) [9,10] in these systems is a key ingredient to stabilize skyrmions. The DMI prefers a chiral magnetic structure, while exchange interaction and Zeeman interaction prefer a uniform structure and they interplay to form a skyrmion/skyrmion lattice. One skyrmion could be represented by a topological charge $q = 1/4\pi \int dxdy\mathbf{S} \cdot (\partial_x \mathbf{S} \times \partial_y \mathbf{S})$, where $\mathbf{S}$ is the unit vector of the spin orientation and the Cartesian coordinates $x - y$ lie in the surface area. The nontrivial topological charge carried by a skyrmion suggests that the skyrmion should be stable against external perturbations, such as the fluctuation of applied fields. Nevertheless, an extremely large field will destabilize the skyrmion structures and align all the spins to form a ferromagnet state; therefore, a skyrmion can only be stabilized at a particular field range in a magnet. For technical applications, the stability window of skyrmions is an important asset since it determines the working window and operational flexibility of the skyrmion-based devices. Here we show the possibility to enlarge the stability window of skyrmions using frustrated exchange interaction.

Frustration in spin systems refers to competing interactions that cannot be satisfied simultaneously and this phenomenon has attracted significant scientific attention in the last few decades due to its unusual ordering properties of the ground states [11–14]. Frustration may come from the geometry of the lattice, such as antiferromagnetically coupled Ising spins on a triangular lattice, and from the competing exchange interactions in a regular lattice, such as a two-dimensional (2D) square lattice with competing nearest-neighbor (NN) (J_1) and next-nearest-neighbor (NNN) exchange interaction (J_2) [15]. To consider the influence of frustrated exchange interaction on the ground-state properties of a chiral system, it is convenient to model the frustrated system as an extended Heisenberg Hamiltonian [16–19] and achieve the ground states via micromagnetic simulations, Monte Carlo simulations, and first-principles calculations. To reproduce the skyrmion phase in an ultrathin film Fe/Ir(111), four-spin exchange interaction and DMI are included in the Heisenberg model and this model successfully explains the reciprocal vector of skyrmion lattice identified by scanning tunneling microscopy [17–19]. According to the simulations, the four-spin interaction plays a crucial role to form skyrmions, but the DMI only makes a difference between skyrmions and antiskyrmions in Fe/Ir(111). Using similar methods, skyrmions are shown to exist in a frustrated system without DMI [20–22]. Indeed, this type of skyrmions stabilized solely by frustration is well studied. Meanwhile, there is another type of system with the coexistence of DMI and frustrated exchange interaction where their strength may be comparable. It is still not known how frustration influences the energy-preferable window of such type of skyrmions. This motivates our current work.

In this paper, we focus on a model with competing exchange interaction and DM interaction in a square lattice and show that the frustrated interaction could enhance the effect of the DMI and then enlarge the energy-preferable window of skyrmions. We also find a multisublattice helical structure that is quite different from the known three-sublattice states observed in an

*Corresponding author: huaiyangyuan@gmail.com

†Corresponding author: helen.gomonay@gmail.com

antiferromagnetic triangular lattice [23]. The phase diagram that contains skyrmions, helical states, and ferromagnetic states is identified. The paper is organized as follows. In Sec. II, the model and numerical method are introduced. In Sec. III, the phase diagram of skyrmions and wasp-waist hysteresis loop are presented, together with detailed analysis. The discussions and conclusions are given in Sec. IV.

II. MODEL AND METHOD

We consider a two-dimensional square lattice where the x, y, and z axes are along the length, width, and thickness directions, respectively. The lateral dimensions of the film are $L \times L$. We consider the magnetic Hamiltonian given by

$$H = -J_1 \sum_{\langle i,j \rangle} \mathbf{S}_i \cdot \mathbf{S}_j + J_2 \sum_{\langle\langle i,j \rangle\rangle} \mathbf{S}_i \cdot \mathbf{S}_j + \sum_{\langle i,j \rangle} \mathbf{D} \cdot \mathbf{S}_i \times \mathbf{S}_j - H \sum_i \mathbf{S}_i^z, \quad (1)$$

where $\mathbf{S}_i$ labels the classical spin orientation at site i, the first and second sums are taken over all NN and NNN pairs, respectively, and J_1, J_2 refer to the corresponding exchange interaction strength. The third term is DMI which results in the stabilization of skyrmions in the lattice and $\mathbf{D}$ is the DM vector. This term is one type of Lifshitz invariant that stabilizes a skyrmion state [2,24,25]. The fourth term is Zeeman energy, where the external field $\mathbf{H}$ is along the thickness direction $(+z)$. A single spin-flip Monte Carlo (MC) method [26] is used to simulate the ground states. To mimic an infinite system, periodic boundary conditions in the x and y directions are used. A typical simulation begins with a completely random state at a sufficient high temperature, $T = 10\ J_1/k_B$, where k_B is Boltzmann constant, and then the system is annealed to a target temperature after at least 10 temperature steps. At each temperature, 10^4 MC steps are taken before measurements are performed. If not stated differently, the grid size $L = 32$ and NN coupling is set to $J_1 = 1.0$.

III. RESULTS

In Sec. III A, we show the stability of a multisublattice helical (MSH) state in the low-field regime and defend that it is a competing result between frustration and DMI. In Sec. III B, we illustrate the phase diagram in the $H - J_2$ plane that includes three distinguishable phases: ferromagnetic (FM) states, skyrmions, and helical states (H), especially the enlarged energy-preferable window (EPW) of the skyrmion phase and helical phase. The expansion of the EPW of skyrmions is attributed to the enhanced DMI in the frustrated system. In Sec. III C, we show and discuss the wasp-waist hysteresis loops and propose to measure the strength of NNN using the characteristic jumps in such a loop.

A. Multisublattice helical state

Figure 1(a) shows the spin configuration of a typical MSH state when $J_2/J_1 = 0.8$ under zero field. The spin orientation is almost uniform in the horizontal direction (x), while it is nonuniform in the vertical direction (y). The state by rotating the spin configuration in Fig. 1(a) by $\pi/2$ around the z direction

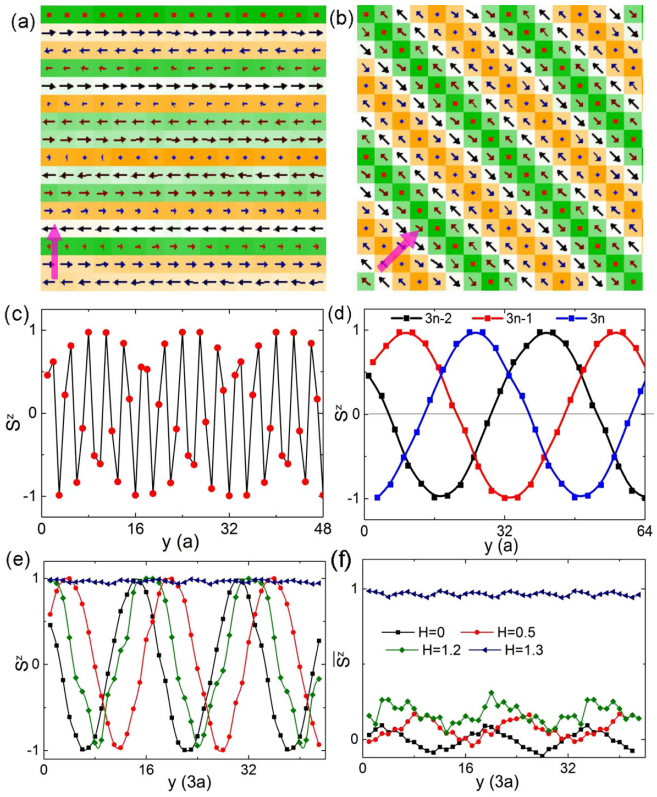

FIG. 1. (a),(b) Ground states of the system for $J_2/J_1 = 0.8$ and 0, respectively, under zero field. The pink arrows indicate the direction of period. The color codes S_z from -1 (green), 0 (white), to $+1$ (orange). (c) S^z as a function of the spin position (y). (d) Replot of $S^z - y$ when the sites are classified into three classes, $i = 3n - 2, 3n - 1, 3n$, where n is a positive integer. $y = ia$, where a is the lattice constant. Black, red, and blue squares represent $3n - 2, 3n - 1, 3n$, respectively. (e) $S^z - y$ for $3n - 2$ sites at various fields in the units of J_1. (f) The average magnetization of the $3n - 2, 3n - 1$, and $3n$ sites $\overline{S^z}$ as a function of unit-cell coordinates (y) for various fields. $\overline{S^z} = (S^z_{3n-2} + S^z_{3n-1} + S^z_{3n})/3$.

is also possible to exist in our system because there is no in-plane anisotropy in our 2D square lattice and the two configurations are energetically degenerate. This MSH state is different from the normal helical state where spins rotate with a fixed chirality in the diagonal direction of the square lattice, as shown in Fig. 1(b). The normal helical state is stable in the regime $J_2/J_1 \leqslant 0.5$ within our model. In the transition region $0.5 < J_2/J_1 < 0.8$, the spin distribution of the ground state is irregular where a curved strip pattern may appear.

To identify the spin arrangements of a MSH state, we plot the z component of a spin (S^z) as a function of spin position in the y direction in Fig. 1(c). Although it shows a periodic behavior with a period of $L_H = 32a$ (a is the lattice constant), it is difficult to recognize the multisublattice chiral structure from this plot directly. Here we introduce a unit cell containing three sublattices with site number $3n - 2$, $3n - 1$, and $3n$, respectively, where n is a positive integer. Figure 1(d) shows the space variation of spins of the three sublattices, respectively. A cosine/sine curve with period $L_H = 48a$ is observed for all three sublattices and a constant phase lag exists for adjacent sublattices. Therefore,

the spin configuration of each sublattice is a normal helical structure, while each unit cell includes three sublattices. That is the reason to name the state as a MSH state. The chirality of the helix in the $+y$ direction is counterclockwise, which is the same as the helical states at small J_2. We defend that the existence of such a multisublattice helical state is the competing result between DMI and exchange coupling. Specifically, when $J_2/J_1 < 0.5$, the NNN coupling is weak, and hence ferromagnetic NN coupling and DMI dominate the other interactions in the system and the ground state is a normal helical state. When $J_2/J_1 > 0.5$, the AFM NNN coupling begins to surpass the ferromagnetic NN coupling and competes with the DMI. Without DMI, the ground state is a two-sublattice Néel state, where spins in a row/column would align ferromagnetically with each other and the spins in a column/row align antiferromagnetically. Once DMI appears, it will prefer a chiral rotation of spins in a particular direction. As a result of this balance, the spins keep their ferromagnetic order in the x direction and change the two-sublattice AFM to a three-sublattice helical state in the y direction. The multisublattice state is very stable as it gains from both the AFM interaction and DMI. It should be noted that one unit cell may contain three, four, and five sublattices in a MSH state, which depends on the strength of frustration.

To see the influence of finite fields on the stability of the MSH state, we anneal the system under different fields and find that the MSH state is still the ground state for fields up to $H/J_1 = 1.3$. Figure 1(e) shows the $S^z - y$ for the $3n-2$ sublattice as we increase the fields (H/J_1) from 0 to 1.3. It shows that the MSH state is stable as the field increases up to 1.2. The phase differences of the $S^z - y$ curves among various fields in Fig. 1(e) are randomly distributed, which is related to the stochastic nature of the spin-flip process in a MC simulation to obtain these states. Nevertheless, as the field increases, the phase difference of the three sites within a unit cell keeps adjusting to increase the average magnetization to gain Zeeman energy, as shown in Fig. 1(f). At the phase boundary $H/J_1 = 1.3$, all the spins in one unit cell tilt along the external field direction such that $\overline{S^z} \approx 1$.

B. Phase diagram

Besides the MSH states and the normal helical states in the low-field regime, the ground state of a frustrated chiral system may be skyrmion lattices in the intermediate-field regime and ferromagnetic domains in the high-field regime. The phase diagram of the ground states in the $HJ_1/D^2 - J_2/J_1$ plane is shown in Fig. 2, where the skyrmion phase and FM phase are denoted as orange and yellow regions, respectively. For $J_2 = 0$, the EPW of the skyrmion phase is $0.24 \leqslant HJ_1/D^2 < 0.73$, which is consistent with literature [1]. When the reduced field is close to 0.73, the density of skyrmions in the lattice decreases and the hexagonal structure of the skyrmion lattice becomes irregular. This observation may be related to the strip-out instability of a skyrmion lattice [25]. With the increase of frustration strength J_2/J_1, the EPW of the skyrmion phase first enlarges and then shrinks, as shown by the orange region in Fig. 2. Up to $J_2/J_1 = 0.9$, the EPW is wider than a frustration-free system ($J_2 = 0$) and the maximum enlargement ratio is 2.2 around $J_2/J_1 = 0.6$. As a comparison, we also simulate

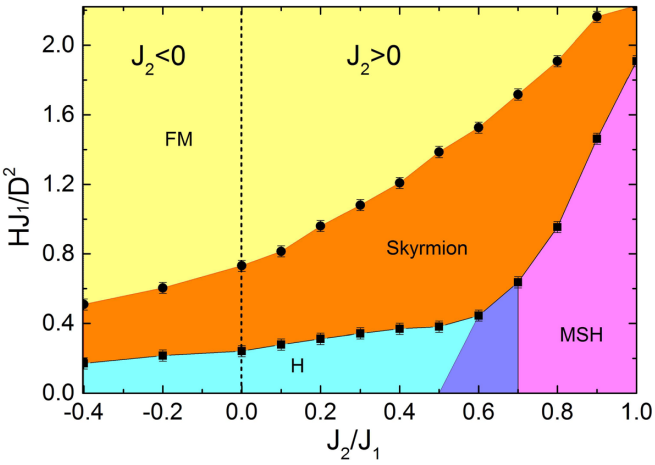

FIG. 2. The calculated phase diagram in the $HJ_1/D^2 - J_2/J_1$ plane. $T = 6.6 \times 10^{-3} J_1/k_B$. The color represents various phases including FM (yellow), skyrmion (orange), H (light blue), transition (dark blue), and MSH (pink). The dashed line refers to $J_2 = 0$.

the case when NNN coupling is ferromagnetic ($J_2 < 0$) and find that the stability region of the skyrmion shrinks. One can check the phase boundary in Fig. 2 by comparing the energy difference between the FM, skyrmions, and helical states [27]. The choice of reference energy to calculate the energy of each state does not influence the position of the phase boundary in Fig. 2.

Now we provide a qualitative understanding of the phase diagram. First, as shown in Fig. 3(a), one spin A has four nearest spins A_{nn} and another four NNN spins A_{nnn}. The

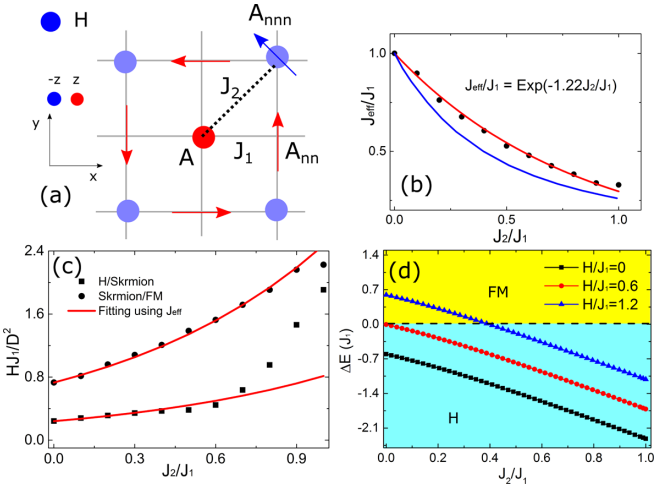

FIG. 3. (a) Scheme of a site A and its neighbors A_{nn}, A_{nnn} on a square lattice. (b) Effective NN exchange J_{eff} as a function of NNN exchange strength. The red line is the fitting curve using the formula $J_{eff}/J_1 = \mathrm{Exp}(-1.22J_2/J_1)$. The blue line is the theoretical prediction. (c) Calculated phase boundary using effective NN coupling J_{eff} (red line) for H/skyrmion ($0.24HJ_{eff}/D^2$) and skyrmion/FM ($0.73HJ_{eff}/D^2$). (d) Energy density difference between a helical state and a FM state calculated from a 1D frustrated model under fields $H/J_1 = 0$ (black square), 0.6 (red dots), and 1.2 (blue up-triangles), respectively. The light blue/yellow region refers to the regions with FM and helix as the ground states, respectively.

introduction of an antiferromagnetic NNN coupling would prefer the spin $A_{\rm nnn}$ to tilt antiparallel to the central spin A. Even though this trend would be suppressed by the ferromagnetic NN coupling between A and $A_{\rm nn}$, it would weaken the NN coupling strength effectively. As a result, the effect of the DMI would be more pronounced and make the skyrmion lattice more energetically favorable. On the other hand, the reduction of the effective exchange coupling would lead to a reduction of the skyrmion size within our simulations [27]. Quantitatively, if it is assumed that the phase boundary between the skyrmion and FM in Fig. 2 still follows the theoretical relation $H_c J_1/D^2 = 0.73$ derived in a frustration-free system [27], with the exchange coupling replaced by an effective exchange coupling that includes the effect of NNN interaction, then the effective coupling $J_{\rm eff}$ as a function of J_2 could be extracted, as shown by the black dots in Fig. 3(b). An exponential fitting $J_{\rm eff}/J_1 = {\rm Exp}(-1.22 J_2/J_1)$ describes the J_2 dependence of $J_{\rm eff}$ well. The effective exchange coupling could well fit the phase boundary between the skyrmion and FM state and the phase boundary between the skyrmion and normal helical state, as shown in the red lines of Fig. 3(c). However, the effective exchange interaction cannot capture the phase boundary between the skyrmion phase and MSH state for $J_2/J_1 > 0.5$. This may be attributed to the pronounced stability of the MSH state, as discussed in Sec. III A.

To further understand the influence of frustration on the chiral states, we consider a frustrated spin chain described by the following Hamiltonian:

$$H = \sum_i \big(- J_1 \mathbf{S}_i \cdot \mathbf{S}_{i+1} + J_2 \mathbf{S}_i \cdot \mathbf{S}_{i+2} - D e_y \cdot \mathbf{S}_i \times \mathbf{S}_{i+1} - H S_i^z \big).$$

The energy density of FM is $E_{\rm FM}/J_1 = -1 + J_2/J_1 - H/J_1$. For the helical state, it is assumed that the spin rotates in the xz plane such that $S_n = (\sin nqa, 0, \cos nqa)$, and the wave vector $q = 2\pi/L_H$, where L_H is the period of the helix. Substituting this trial function S_n into the Hamiltonian and minimizing the total energy gives a quartic polynomial equation,

$$Dx^4 + (2J_1 + 4J_2)x^3 + (2J_1 - 4J_2)x - D = 0,$$

where $x = \tan(qa/2)$. For $J_2 = 0$, the solution is $J_1 \tan(qa) = D$, which is consistent with the literature [28]. For $J_2 \neq 0$, the quartic solution has a positive real root (q_0), which indicates the existence of a helical structure. Substituting this root (q_0) back to the Hamiltonian, we could calculate the energy of the helix. Figure 3(d) shows the energy density difference between the helical state and FM state as a function of J_2/J_1. For $H/J_1 < 0.6$, the energy of the helix is always smaller than the energy of the FM state; hence the ground state of the system is a helix. For $H/J_1 > 0.6$, the helix is energetically preferred in the larger J_2/J_1 regime, while the FM is energetically preferred in the smaller J_2/J_1 regime. By fitting the phase boundary between the helix and FM state in the parameter space $H - J_2$ using an effective exchange constant $J_{\rm eff}$, we could extract $J_{\rm eff}$ as a function of J_2/J_1 in the frustrated system, as shown in the blue line of Fig. 3(b). The theoretical curve in the one-dimensional (1D) model (blue line) could roughly capture the trend of numerical results (black dots) in the simulations.

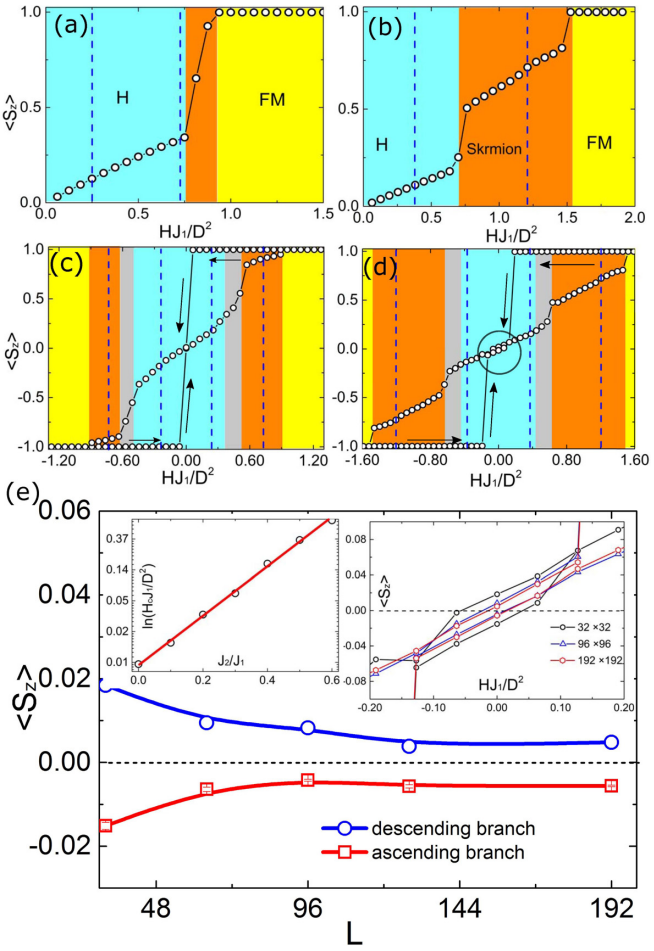

FIG. 4. First magnetization curves for (a) $J_2 = 0$ and (b) $J_2 = 0.4$, and hysteresis loops for (c) $J_2/J_1 = 0.0$ and (d) 0.4. $\langle S_z \rangle$ is defined as $\langle S_z \rangle = 1/L^2 \sum_i S_i^z$. Blue: helix; orange: skyrmion; yellow: FM state; gray: mixing of helix and skyrmion. (e) is the enlarged figure of the circled part in (d). $T = 6.6 \times 10^{-3}$ J$_1$/k$_{\rm B}$, $L = 32$. (e) $\langle S_z \rangle$ as a function of sample size for the descending branch (blue circles) and ascending branch (red squares), respectively. The left inset is the critical field H_c as a function of J_2/J_1. The right inset is the size effect of the hysteresis loop at small fields for $L = 32$ (black circles), 96 (blue triangles), and 192 (red hexagons), respectively.

C. Hysteresis loop

In this section, we investigate the shape of the hysteresis loop in a frustrated chiral system. The thermal effect is suppressed by considering a system at sufficiently low temperature, $T = 6.67 \times 10^{-3}$ J$_1$/k$_{\rm B}$. Figures 4(a) and 4(b) show the first magnetization curves. The average magnetization is defined as $\langle S_z \rangle = 1/L^2 \sum_i S_i^z$. To simulate the first magnetization curve, we start from a helical state obtained from an annealing process under $H = 0$ and then increase the field in the step of $0.1 J_1/D^2$. For $J_2 = 0$, the helical phase is stable up to $H J_1/D^2 = 0.76$ and the skyrmion phase only exists in a narrow window for $0.76 < H J_1/D^2 < 0.95$, as shown in Fig. 4(a). For $J_2 = 0.4$, the skyrmion is stable at the range $0.70 < H J_1/D^2 < 1.52$, which is significantly larger than the window at $J_2 = 0$. For both $J_2 = 0$ and $J_2 = 0.4$, the stability regime of the skyrmion phase is different from the

phase diagram shown in Fig. 2, which is due to the hysteretic nature of a magnetic system. The final spin configuration depends sensitively on the evolution history, even though the initial states are the same. At a fixed low temperature ($6.67 \times 10^{-3}\ J_1/k_B$), the thermal energy is too small for the system to overcome the energy barrier to reach a skyrmion state unless a sufficiently large field is applied such that the energy barrier is substantially lowered. As a comparison, the annealing procedure used to obtain the phase diagram in Fig. 2 is more efficient to reach the real global minimum states of the system because sufficient energy is provided to the spins to overcome the energy barrier between the skyrmion and H/FM.

Figures 4(c) and 4(d) show the hysteresis loops for $J_2 = 0$ and $J_2 = 0.4$, respectively. To simulate the hysteresis loop, we start from a FM state obtained by annealing procedures at high fields and then decrease the fields in the step of $0.1J_1/D^2$ to obtain the descending branch, and then reverse the direction of the fields to get the ascending branch. Both of the hysteresis loops in Figs. 4(c) and 4(d) take on a wasp-waist shape, where the loop shrinks as the magnetization goes to zero and then opens up again. The field that separates the wide and narrow parts of the hysteresis loop is denoted as the critical field (H_c). The critical field is $H_c = 0$ for $J_2 = 0$, while it is at $H_c = 0.16D^2/J_1$ for $J_2 = 0.4$, as shown in Figs. 4(c) and 4(d). To clearly see the shape of the loops in the small magnetization regime and understand the role of the finite-size effect in the simulations, we vary the system size as $L = 32, 64, 96, 128, 192$ and plot all the L dependence of the magnetization for the ascending branch and descending branch at zero field in Fig. 4(e). The gap between the two branches decreases gradually to a constant. Therefore, it is expected that the loop at smaller fields would result in two closely parallel branches as $L \to \infty$.

To understand the wasp-waist hysteresis, we refer to the scheme in Fig. 3(a). As we reduce the fields slowly from a high-field value, the system first stabilizes at a FM state, where spins at A and its neighbors A_{nn} and A_{nnn} (almost) align in the $+z$ direction. Similar to the arguments for the first magnetization curves, even though the skyrmion/helical states are the global minimum states for $HJ_1/D^2 < 0.76$, the FM states ($q = 0$) and skyrmions ($q = \pm 1$) are topologically different [29,30], where the transformation between them needs to overcome a finite-energy barrier. As the temperature is low, the rotation degrees of freedom for the spins are frozen and this makes the system difficult to climb across the barrier to reach a lower-energy state. When antiferromagnetic NNN coupling is present, the spins between A_{nn} and A will tend to align antiparallel to each other, which will destabilize the FM state and lower the energy barrier between the FM and helical states. That is why the critical field becomes finite. According to this argument, the larger the NNN coupling (J_2), the lower the barrier between the FM and helical states; hence the larger the critical field. The left inset in Fig. 4(e) demonstrates this argument and further shows that the critical field increases almost exponentially with the increase of J_2. This also provides a method to characterize the strength of NNN coupling in a ferromagnetic film by measuring the critical field in the wasp-waist hysteresis loop.

IV. DISCUSSIONS AND CONCLUSIONS

First, we compare our results with the known literature. Skyrmions and helical states in an antiferromagnetic triangular lattice are found to consist of three interpenetrating sublattices [23]. The three-sublattice structure of the chiral states results from the three-sublattice nature of the antiferromagnetic triangular lattice and the authors also expect that the spins have the tendency to form a two-sublattice structure in a square lattice, which is quite different from the frustrated square lattice we considered here. The skyrmion lattice in our model does not have a multisublattice structure, while the helical states in our model can consist of three, four, and five sublattices, which depend on the strength of frustration. Another literature studied the chiral states in an AFM square lattice and found that the conventional skyrmion lattice is absent in the system [31], which is also different from our results. The difference also shows that the chiral states in a AFM square lattice and frustrated square lattice are different.

Second, we would like to mention that a similar wasp-waist hysteresis loop was experimentally observed in Co/Pt multilayer structures with low disorder [32]. At the critical field in which magnetization decreases significantly, a labyrinthlike magnetic pattern was observed. Another system that allows for the wasp-waist loop is a chiral system with in-plane easy-axis anisotropy [33]. The critical field of the hysteresis loop depends on the in-plane anisotropy strength. One should be careful to clarify the source of the critical field when NNN coupling and easy-axis anisotropy are possible to coexist in a system.

In conclusion, we have studied the existence and the energy-preferable window of chiral states in a frustrated magnet. The AFM NNN interaction diminishes the FM NN interaction to a certain degree and the DMI becomes more pronounced; hence both the helical states and skyrmions could be stabilized in an even larger window compared to a system without frustration. As the stability window of skyrmions is the key to fabricating skyrmion-based devices, our results may be relevant for applications. The theory based on the effective ferromagnetic exchange could quantitatively capture the phase boundary among skyrmions, FM states, and the helix, except for the skyrmion/helix boundary when the AFM coupling is larger than half of the FM coupling. In this regime, a multisublattice helical state instead of a conventional helical state exists below the skyrmion phase. The multisublattice state gains both AFM and DM energy and is energetically preferable up to high fields. Moreover, the hysteresis loop of the chiral frustrated system takes on a wasp-waist shape and the critical field at which the loop shrinks depends on the strength of NNN coupling. By measuring the critical field, it is possible to determine the strength of NNN coupling. It is known that the exchange coupling of Fe could be both ferromagnetic and antiferromagnetic, which depends on the substrates' d-band filling [14,34,35]. Recently, an *ab initio* calculation showed that ferromagnetic NN and AFM NNN interaction could coexist in some multilayer structures such as $Pt_{1-x}Ir_x$/Fe/Pd [36], where our simulation results are promising to be verified experimentally.

ACKNOWLEDGMENTS

We acknowledge the significant discussions with Bertrand Dupé and the helpful comments from Jairo Sinova and Alex Bogdanov. We acknowledge the support from Deutsche Forschungsgemeinschaft (DFG) via the Transregional Collaborative Research Center (SFB/TRR) 173 "Spin+X - Spin its collective environment" and the ERC Synergy Grant SC2 (Grant No. 610115). H.Y.Y. is partially supported by the National Natural Science Foundation of China (Grant No. 61704071).

[1] J. Iwasaki, M. Mochizuki, and N. Nagaosa, Nat. Commun. **4**, 1463 (2013).
[2] A. N. Bogdanov and D. A. Yablonskiĭ, Zh. Eksp. Teor. Fiz. **95**, 178 (1989) [Sov. Phys. JETP **68**, 101 (1989)].
[3] A. N. Bogdanov and U. K. Rößler, Phys. Rev. Lett. **87**, 037203 (2001).
[4] U. K. Rößler, A. N. Bogdanov, and C. Pfleiderer, Nature (London) **442**, 797 (2006).
[5] S. Mühlbauer, B. Binz, F. Jonietz, C. Pfleiderer, A. Rosch, A. Neubauer, R. Georgii, and P. Böni, Science **323**, 915 (2009).
[6] X. Z. Yu, Y. Onose, N. Kanazawa, J. H. Park, J. H. Han, Y. Matsui, N. Nagaosa, and Y. Tokura, Nature (London) **465**, 901 (2010).
[7] X. Z. Yu *et al.*, Nat. Mater. **10**, 106 (2011).
[8] S. Woo *et al.*, Nat. Mater. **15**, 501 (2016).
[9] I. E. Dzyaloshinskii, J. Exptl. Theoret. Phys. (U.S.S.R.) **32**, 1547 (1957) [Sov. Phys. JETP **5**, 1259 (1957)].
[10] T. Moriya, Phys. Rev. **120**, 91 (1960).
[11] G. H. Wannier, Phys. Rev. **79**, 357 (1950).
[12] L. G. Marland and D. D. Betts, Phys. Rev. Lett. **43**, 1618 (1979).
[13] J. T. Chalker, P. C. W. Holdsworth, and E. F. Shender, Phys. Rev. Lett. **68**, 855 (1992).
[14] B. Hardrat, A. Al-Zubi, P. Ferriani, S. Blügel, G. Bihlmayer, and S. Heinze, Phys. Rev. B **79**, 094411 (2009).
[15] J. Stephenson, Phys. Rev. B **1**, 4405 (1970).
[16] P. Kurz, G. Bihlmayer, S. Blügel, K. Hirai, and T. Asada, Phys. Rev. B **63**, 096401 (2001).
[17] S. Heinze, K. von Bergmann, M. Menzel, J. Brede, A. Kubetzka, R. Wiesendanger, G. Bihlmayer, and S. Blügel, Nat. Phys. **7**, 713 (2011).
[18] B. Dupé, M. Hoffmann, C. Paillard, and S. Heinze, Nat. Commun. **5**, 4030 (2014).
[19] B. Dupé, G. Bihlmayer, M. Böttcher, S. Blügel, and S. Heinze, Nat. Commun. **7**, 11779 (2016).
[20] T. Okubo, S. Chung, and H. Kawamura, Phys. Rev. Lett. **108**, 017206 (2012).
[21] A. O. Leonov and M. Mostovoy, Nat. Commun. **6**, 8275 (2015).
[22] S. Hayami, S.-Z. Lin, and C. D. Batista, Phys. Rev. B **93**, 184413 (2016).
[23] H. D. Rosales, D. C. Cabra, and P. Pujol, Phys. Rev. B **92**, 214439 (2015).
[24] Y. A. Izyumov, Usp. Fiz. Nauk **144**, 439 (1984) [Sov. Phys. Usp. **27**, 845 (1984)].
[25] A. O. Leonov, T. L. Monchesky, N. Romming, A. Kubetzka, A. N. Bogdanov, and R. Wiesendanger, New J. Phys. **18**, 065003 (2016).
[26] N. Metropolis, A. W. Rosenbluth, M. N. Rosenbluth, A. H. Teller, and E. Teller, J. Chem. Phys. **21**, 1087 (1953).
[27] J. H. Han, J. Zang, Z. Yang, J.-H. Park, and N. Nagaosa, Phys. Rev. B **82**, 094429 (2010).
[28] S. D. Yi, S. Onoda, N. Nagaosa, and J. H. Han, Phys. Rev. B **80**, 054416 (2009).
[29] H. Y. Yuan and X. R. Wang, Sci. Rep. **6**, 22638 (2016).
[30] Y. Zhou and M. Ezawa, Nat. Commun. **5**, 4652 (2014).
[31] R. Keesman, M. Raaijmakers, A. E. Baerends, G. T. Barkema, and R. A. Duine, Phys. Rev. B **94**, 054402 (2016).
[32] M. S. Pierce, C. R. Buechler, L. B. Sorensen, S. D. Kevan, E. A. Jagla, J. M. Deutsch, T. Mai, O. Narayan, J. E. Davies, K. Liu, G. T. Zimanyi, H. G. Katzgraber, O. Hellwig, E. E. Fullerton, P. Fischer, and J. B. Kortright, Phys. Rev. B **75**, 144406 (2007).
[33] H. Y. Kwon, K. M. Bu, Y. Z. Wu, and C. Won, J. Magn. Magn. Mater. **324**, 2171 (2012).
[34] L. Rózsa, L. Udvardi, L. Szunyogh, and I. A. Szabó, Phys. Rev. B **91**, 144424 (2015).
[35] L. Rózsa, E. Simon, K. Palotás, L. Udvardi, and L. Szunyogh, Phys. Rev. B **93**, 024417 (2016).
[36] L. Rózsa, A. Deák, E. Simon, R. Yanes, L. Udvardi, L. Szunyogh, and U. Nowak, Phys. Rev. Lett. **117**, 157205 (2016).